General Conditions to Realize Exceptional Points of Degeneracy in Two Uniform Coupled Transmission Lines

Tarek Mealy and Filippo Capolino, *Fellow, IEEE*

***Abstract*— We present the general conditions to realize a fourth-order exceptional point of degeneracy (EPD) in two *uniform* (i.e., invariant along z) lossless and gainless coupled transmission lines (CTLs), namely, a degenerate band edge (DBE). Until now the DBE has been shown only in periodic structures. In contrast, the CTLs considered here are uniform and subdivided into four cases where the two TLs support combinations of forward propagation, backward propagation, and evanescent modes (when neglecting the mutual coupling). We demonstrate, for the first time, that a DBE is supported in *uniform* CTLs when there is proper coupling between: 1) propagating modes and evanescent modes, 2) forward and backward propagating modes, or 3) four evanescent modes (two in each direction). We also show that the loaded quality factor of *uniform* CTLs exhibiting a fourth-order EPD at $k = 0$ is robust to series losses due to the fact that the degenerate modes do not advance in phase. We also provide a microstrip possible implementation of a uniform CTL exhibiting a DBE using periodic series capacitors with very subwavelength unit-cell length. Finally, we show an experimental verification of the existence DBE for a microstrip implementation of a CTL supporting coupled propagating and evanescent modes.**

***Index Terms*— Bandgaps, coupled transmission line (CTL), critical point, degeneracies, exceptional point of degeneracy (EPD), uniform structures, waveguides.**

I. Introduction

EXCEPTIONAL points of degeneracy (EPDs) are points in parameter space where two or more eigenmodes of a waveguide coalesce into a single eigenmode. The dispersion relation of eigenmodes in a waveguide that exhibits an EPD with order m, where m is the number of coalescing eigenmodes, has the behavior of $(\omega-\omega_e) \propto (k-k_e)^m$ near the EPD at (ω_e, k_e) [1], [2]. Here, ω and k are the angular frequency and the wavenumber, respectively, and the EPD is denoted by the subscript e. Such dispersion behavior is accompanied by a severe reduction in the group velocity of waves propagating in those structures and a tremendous increase in local density of states [3] resulting in a giant increase in the loaded quality factor of the structure [4], [5]. Indeed for a lossless waveguide exhibiting an EPD of order m not only the group velocity $v_g = \partial\omega/\partial k$ vanishes, but all of its derivatives $\partial v_g^i/\partial k^i$ with $i < m-1$ vanish as well [6].

In general, EPDs occur in coupled resonator systems and in coupled-multimode waveguides. Recently, the occurrence of EPDs has been shown in a *single* resonator where one of its elements is time modulated [7]. In this article, we focus on EPDs occurring in multimode waveguides. Furthermore, there are a few types of EPDs, some involve the simultaneous presence of loss and gain, like in parity time (PT) symmetric systems [8], [9]. Here, however, we focus on EPDs that do not require loss and gain to occur, namely we focus on the regular band edge (RBE) and on the degenerate band edge (DBE), that is a fourth-order EPD introduced a few years ago by Figotin and Vitebskiy in layered anisotropic crystals [1], [4].

Recent work has shown that the DBE can be engineered in various types of *periodic* guiding systems. The DBE is a fourth-order EPD existing in periodic waveguides without loss and gain. It has been shown to exist in photonic crystals [1], [3], [10], circular waveguides with periodic inclusions [11], two coupled substrate integrated waveguides [12], two coupled periodic transmission lines [13], [14], ladder circuits [15], and integrated coupled optical waveguides [2], [16]. The first experimental demonstration of the existence of the DBE in periodic waveguides at radio frequency was shown in [17], and recently extended to periodic coupled microstrips [18]. Structures exhibiting DBEs have been proposed recently for a wide range of applications such as, for example, high quality factors photonic crystals [5], high power electron-beam devices [19], [20], RF oscillators [21], and lasers [22].

There are only a few ways to obtain EPDs in *uniform* waveguides. The simplest second-order EPD is found in uniform waveguides at the modal cutoff frequency where two modes, the forward and backward modes, coalesce at $k = 0$, forming an EPD of order 2 that is called "regular" band edge [23]. Another way to realize second-order EPDs in *uniform* coupled transmission lines (CTLs) is based on PT-symmetry [8], [24] which implies using a balanced and symmetrical distribution of gain and loss [9]. In contrast to these two types of second-order EPD, in this article we show there are other ways to realize EPDs of fourth order in two lossless/gainless *uniform* CTLs at $k = 0$. Therefore, this article shows for the first time how to realize a DBE at $k = 0$ in uniform transmission lines (Fig. 1) since previously the DBE was

Manuscript received March 13, 2020; revised May 13, 2020; accepted May 22, 2020. Date of publication June 15, 2020; date of current version August 5, 2020. This work was supported in part by the Air Force Office of Scientific Research under Award FA9550-15-1-0280 and Award FA9550-18-1-0355 and in part by the National Science Foundation under Grant NSF ECCS-1711975. *(Corresponding author: Filippo Capolino.)*

The authors are with the Department of Electrical Engineering and Computer Science, University of California at Irvine, Irvine, CA 92697 USA (e-mail: tmealy@uci.edu; f.capolino@uci.edu).

Color versions of one or more of the figures in this article are available online at http://ieeexplore.ieee.org.

Digital Object Identifier 10.1109/TMTT.2020.2999498

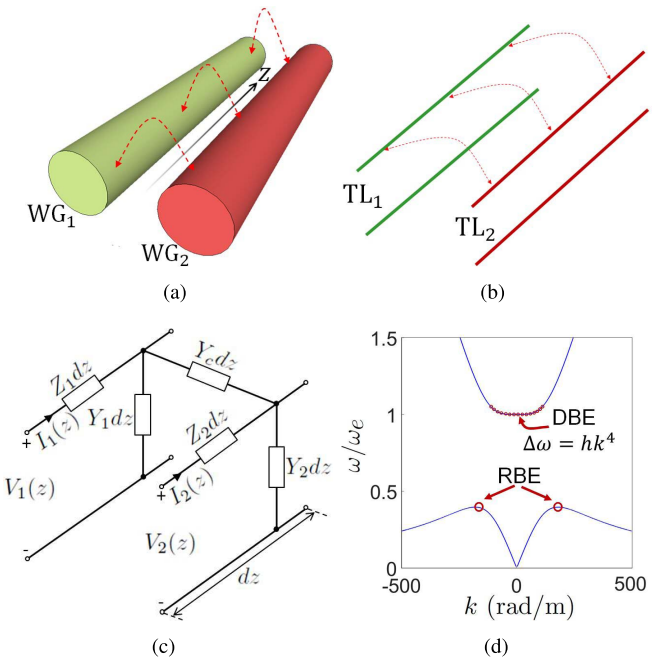

Fig. 1. (a) Two uniform coupled waveguides supporting four modes (two in each direction). Modes have wavenumbers satisfying the k and $-k$ symmetry, due to reciprocity. (b) Equivalent CTL model describing the propagation of the four modes in the two uniform coupled waveguides. (c) Generalized per-unit-length distributed equivalent circuit model for the CTL. Coupling is represented by the distributed (i.e., per-unit-length) admittance Y_c. In this article, we determine the necessary and sufficient conditions that the five reactances shall satisfy for the CTLs to exhibit a DBE, that is, a fourth-order degeneracy. (d) Representation of a dispersion diagram (showing only the branches of purely real wavenumber) reporting two important features: the DBE at $k_e = 0$ and $\omega = \omega_e$ (that is a fourth-order EPD), and an RBE at $\omega = 0.4\omega_e$, with a nonvanishing wavenumber of $k = \pm 147.5$ rad/m (a second-order EPD).

shown only in periodic waveguides [1], [2], [11], [16], [18]. This article also shows how to locate an RBE (an EPD of order 2) at any k, in *uniform* waveguides (Fig. 1).

In Section II, we discuss briefly all possible EPDs that may exist in two *uniform* CTLs, and their general necessary and sufficient conditions. In Section III, we show the necessary and sufficient conditions to realize fourth-order EPD in two uniform, lossless, CTLs in terms of their per-unit-length parameters, and we show all possible typologies that may support a fourth-order EPD, namely a DBE, at $k = 0$. We also show that CTLs of finite length make formidable resonators that exhibit an L^5 scaling of the quality factor with the CTL length L. Finally, we show the effect of CTL losses on the occurrence of the DBE and on the quality factor and show that series losses affect the DBE much less than shunt losses. In Section IV, we present an example of *uniform* CTLs that support a DBE at $k = 0$ and we also provide a microstrip possible implementation of such uniform CTLs exhibiting the DBE using a series per-unit-length inductance realized with a very subwavelength unit-cell length. In Section V, we show two experimental validations of the occurrence of the DBE in uniform CTLs, using periodic capacitive loading with subwavelength period, approximating (in a metamaterials sense) the uniform CTL. The findings in this article open up new ways to conceive distributed oscillators, leaky wave antennas, and radiating leaky wave antennas with extreme tunability, waveguide-based sensors, etc.

II. System Description of Uniform Coupled Waveguides

Consider the two *uniform* waveguides schematically shown in Fig. 1(a), where each waveguide (when uncoupled) supports either a forward propagating mode, a backward propagating mode (where group velocity and phase velocity have opposite sign) or an evanescent mode; along each positive and negative z-direction due to reciprocity.

An equivalent CTL model is used to describe the coupled waveguides in Fig. 1(a) [25], [26] and this model can also be used to describe propagation in several other "two-ways" guiding geometries that support two waves in each direction. Let V_n and I_n, with $n = 1, 2$, respectively, be the equivalent voltage and current in each TL of Fig. 1(b), describing the spatial evolution of electromagnetic waves along the z-direction. It is convenient to introduce the 2-D vectors $\mathbf{V}(z) = [\, V_1(z) \;\; V_2(z) \,]^{\mathrm{T}}$, $\mathbf{I}(z) = [\, I_1(z) \;\; I_2(z) \,]^{\mathrm{T}}$, where the superscript T represents the transpose operation.

When the two transmission lines are not coupled they support four independent modes that are described by four distinct wavenumbers k_1', k_2' and $-k_1'$, $-k_2'$ and their voltage and current are written as

$$V_n(z) \propto e^{\pm jk_n' z}, \quad I_n(z) \propto e^{\pm jk_n' z} \tag{1}$$

where the modal wavenumbers k_n', with $n = 1, 2$, are generally written as $k_n' = \beta_n - j\alpha_n$, where β_n and α_n are the phase propagation and attenuation constants, respectively, and they determine the type of mode; for example, a wavenumber k' that possesses only the imaginary part α is an evanescent mode. Forward modes are determined by $\beta\alpha > 0$, whereas "backward" propagating modes have $\beta\alpha < 0$ (hence, backward propagating modes have phase and group velocities with opposite directions).

The circuit *equivalent* model for an infinitesimal-length of a waveguide is represented by generic per-unit-length distributed parameters as shown in Fig. 1(c). There, Z_1, Z_2, Y_1, Y_2, and Y_c may be inductive or capacitive impedances and admittances. In this article, for the sake of brevity, we do not consider magnetic induction coupling between the two TLs, that is, we consider only shunt per-unit-length inductive or capacitive coupling Y_c shown in Fig. 1(c). Coupling due to magnetic induction between two nearby lines could be investigated using the same mechanism and formulation used in this article and it is not treated here. It can be neglected in several cases, when the separation between the two lines is very large, for examples, or for the case studied in Section IV, where the coupling is due to the physical connection between the first and second TL.

We assume that Z_1 and Z_2 may be either capacitive or inductive impedances, as well as Y_1 and Y_2 can be either capacitive or inductive, where the subscripts 1 and 2 are used to describe the parameters in the first and second transmission lines TL_1 and TL_2, respectively. We recall that a single TL (say TL_1 for example) supports backward waves if Z_1 is capacitive

and Y_1 is inductive. Furthermore, a TL (say TL_1, for example) supports evanescent waves if both Z_1 and Y_1 have the same kind of reactance. An example of dispersion diagram with a DBE (a fourth-order EPD) at $k = 0$ and a RBE (a second-order EPD) at $k \neq 0$, is shown in Fig. 1(d), using the CTL parameters provided in Section III. The DBE occurring at $k = 0$, which is the main focus of this article, has a dispersion characterized by the relation [1], [2]

$$(\omega - \omega_e) = hk^4 \tag{2}$$

in the vicinity of $k = 0$, where h is a geometry-dependent fitting parameter that controls the flatness of the dispersion.

Using the matrix notation as in [27] for the circuit *equivalent* model in Fig. 1(c), the differential wave equations (telegrapher's equations) describing propagation in the two CTLs are

$$\begin{aligned} \frac{d\mathbf{V}(z)}{dz} &= -\underline{\underline{\mathbf{Z}}}(\omega)\mathbf{I}(z) \\ \frac{d\mathbf{I}(z)}{dz} &= -\underline{\underline{\mathbf{Y}}}(\omega)\mathbf{V}(z). \end{aligned} \tag{3}$$

Here, $\underline{\underline{\mathbf{Z}}}$ and $\underline{\underline{\mathbf{Y}}}$ are the per-unit-length series-impedance and shunt-admittance matrices, respectively, describing the per-unit-length distributed parameters of the CTLs [27]. They are 2×2 symmetric matrices given by

$$\begin{aligned} \underline{\underline{\mathbf{Z}}}(\omega) &= \begin{pmatrix} Z_1(\omega) & 0 \\ 0 & Z_2(\omega) \end{pmatrix} \\ \underline{\underline{\mathbf{Y}}} &= \begin{pmatrix} Y_1(\omega) + Y_c(\omega) & -Y_c(\omega) \\ -Y_c(\omega) & Y_2(\omega) + Y_c(\omega) \end{pmatrix} \end{aligned} \tag{4}$$

where the coupling between the two TLs is due to $Y_c(\omega)$. For the sake of convenience, a 4-D state vector that includes voltages and currents at a coordinate z in the CTLs is defined as

$$\Psi(z) = \left[V_1(z), \quad V_2(z), \quad I_1(z), \quad I_2(z) \right]^{\mathrm{T}}. \tag{5}$$

Therefore, the two telegrapher equations (3) representing wave propagation are cast in terms of a multidimensional first-order differential equation [9], [28]

$$\frac{d\Psi(z)}{dz} = -j\underline{\mathbf{M}}(\omega)\Psi(z) \tag{6}$$

where $\underline{\mathbf{M}}(\omega)$ is a 4×4 system matrix given by

$$\underline{\mathbf{M}}(\omega) = \begin{pmatrix} \underline{\underline{\mathbf{0}}} & -j\underline{\underline{\mathbf{Z}}}(\omega) \\ -j\underline{\underline{\mathbf{Y}}}(\omega) & \underline{\underline{\mathbf{0}}} \end{pmatrix} \tag{7}$$

and $\underline{\underline{\mathbf{0}}}$ is the 2×2 null matrix.

When the matrix $\underline{\mathbf{M}}(\omega)$ is diagonalizable all the four eigenmodes supported in the CTL have state vectors $\Psi_n(z) \propto e^{-jk_n z}$, with $n = 1, 2, 3, 4$, see proof in Appendix A; however, when the matrix $\underline{\mathbf{M}}(\omega)$ is not diagonalizable (this is corresponding to the case exhibiting an EPD), some modes preserve the proportionality $\Psi_n(z) \propto e^{-jk_n z}$, while the rest have algebraic growth with z as $\Psi_n \propto \mathbf{P}(z)e^{-jk_n z}$, where $\mathbf{P}(z)$ is a vector polynomial function of maximum order 3 for systems made of two CTLs as considered in this article, see proof in Appendix A. Therefore, when $\underline{\mathbf{M}}(\omega)$ is diagonalizable the eigenmodes supported by the uniform CTL described by (6) are fully represented by using $\Psi(z) \propto e^{-jkz}$ in (6) to obtain $-jk\,\Psi(z) = -j\underline{\mathbf{M}}(\omega)\Psi(z)$ [9], yet simplified to an eigenvalue problem as

$$\underline{\mathbf{M}}\Psi(z) = k\Psi(z). \tag{8}$$

The four eigenvalues k_1, k_2, k_3 and k_4 and their corresponding eigenvectors (at $z = 0$) Ψ_1, Ψ_2, Ψ_3, and Ψ_4 of the above eigenvalue problem are determined as in Appendix B and they are written in their simplest form as [28]

$$\begin{aligned} k_1 &= -k_3 = \frac{1}{\sqrt{2}}\sqrt{-T - \sqrt{T^2 - 4\mathrm{D}}} \\ k_2 &= -k_4 = \frac{1}{\sqrt{2}}\sqrt{-T + \sqrt{T^2 - 4\mathrm{D}}} \end{aligned} \tag{9}$$

where $T = \mathrm{Tr}(\underline{\underline{\mathbf{Z}}}\ \underline{\underline{\mathbf{Y}}})$ is the trace and $D = \det(\underline{\underline{\mathbf{Z}}}\ \underline{\underline{\mathbf{Y}}})$. The system vector is concisely and conveniently represented as

$$\Psi_n = \psi_0 \begin{pmatrix} Z_1\left(k_n^2 + Z_2(Y_2 + Y_c)\right) \\ Z_1 Z_2 Y_c \\ jk_n\left(k_n^2 + Z_2(Y_2 + Y_c)\right) \\ jZ_1 k_n Y_c \end{pmatrix} \tag{10}$$

where ψ_0 is arbitrary constant and it has a unit of Am^3.

The solutions (9) and (10) represent the four wavenumbers of the eigenmodes that propagate or attenuate along both the positive and negative z-directions (four modes), viz., $k_3 = -k_1$ and $k_4 = -k_2$.

In general, an EPD of order m occurs when m eigenomodes have the same eigenvalue and eigenvector. For a system of two uniform CTLs a fourth-order EPD (a full order EPD) occurs if all the 4 eigenvalues are equal [28], which implies that eigenvectors coalesce as well, as it is obvious from (10). Therefore, in such a uniform system the coalescence of four wavenumbers is a sufficient condition for an EPD to occur.

The system made of two CTLs considered in this article exhibits three types of EPDs: 1) two points of second-order degeneracy ($k_1 = k_2$ and $k_3 = k_4$) when $T^2 = 4\mathrm{D}$. This can occur at any wavenumber k; 2) a second-order EPD ($k_1 = k_3$) or ($k_2 = k_4$) when $D = 0$. This occurs only at $k = 0$; and 3) a fourth-order EPD ($k_1 = k_2 = k_3 = k_4$) when both $T = 0$ and $D = 0$. This occurs only at $k = 0$. These three cases are illustrated in the dispersion diagram in Fig. 2 and in the schematic representation of the four eigenvectors in Fig. 3. Indeed, in a reciprocal systems ($k_1 = -k_3$), the equality ($k_1 = k_3$) in condition 2) implies that ($k_1 = k_3 = 0$). Furthermore, still based on reciprocity, the condition ($k_1 = k_2 = k_3 = k_4$) in 3) implies that ($k_1 = k_2 = k_3 = k_4 = 0$). Hence, these two conditions can also be used also to design systems radiating at broadside and working at an EPD. Condition 2) is usually referred to as a cutoff condition (at $k = 0$) and indeed it occurs also in regular single mode waveguides. Condition 1) is interesting, because it sets a cutoff condition at any desired wavenumber $k \neq 0$. It is important to point out that a third-order EPD cannot exist in two CTLs unless reciprocity is broken [29] which is out of the scope of this article; here we only consider reciprocal CTLs. The scope of this article is mainly to show the fourth-order degeneracy (namely the DBE) described in condition 3) and to show that condition 1) can also be easily engineered.

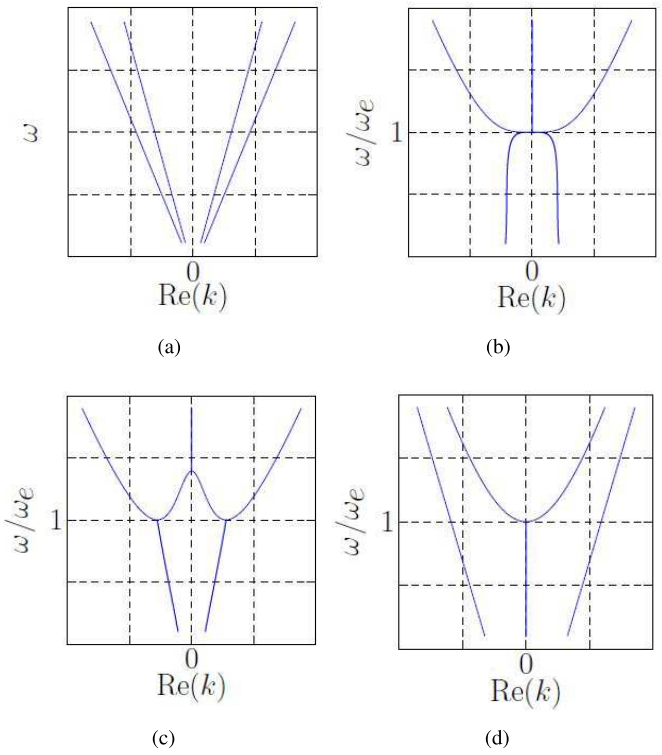

Fig. 2. Dispersion diagrams describing different EPDs at angular frequency ω_e. (a) CTLs where none of the EPD conditions are satisfied at any nonzero frequency. (b) CTLs exhibiting the fourth-order EPD (i.e., the DBE) at the angular frequency ω_e where $\mathrm{Tr}(\underline{\underline{\mathbf{Z}}}(\omega_e)\underline{\underline{\mathbf{Y}}}(\omega_e)) = 0$ and $\det(\underline{\underline{\mathbf{Z}}}(\omega_e)\ \underline{\underline{\mathbf{Y}}}(\omega_e)) = 0$. For uniform CTLs made of 2 TLs this condition necessarily occurs at $k = 0$. (c) CTLs exhibiting two exceptional points of second-order degeneracy, where $\mathrm{Tr}(\underline{\underline{\mathbf{Z}}}(\omega_e)\underline{\underline{\mathbf{Y}}}(\omega_e))^2 = 4\det(\underline{\underline{\mathbf{Z}}}(\omega_e)\ \underline{\underline{\mathbf{Y}}}(\omega_e))$. For uniform CTLs made of two TLs this can occur at any k. (d) CTLs exhibiting a single second-order EPD where $\det(\underline{\underline{\mathbf{Z}}}(\omega_e)\ \underline{\underline{\mathbf{Y}}}(\omega_e)) = 0$. This condition occurs at $k = 0$. In these plots, we show only the real part of the four modal wavenumbers.

III. Fourth-Order DBE in Uniform Waveguides

When modes are supported in uniform waveguides modeled by two uniform and coupled TLs, a fourth-order EPD (DBE) occurs when all four independent eigenvectors coalesce and form one single eigenvector [1], [6] as schematically shown in Fig. 3(b). This occurs when the impedance and admittance matrices that describe the per-unit-length parameters of the system satisfy both conditions

$$T = \mathrm{Tr}\left(\underline{\underline{\mathbf{Z}}}\ \underline{\underline{\mathbf{Y}}}\right) = 0$$
$$D = \det\left(\underline{\underline{\mathbf{ZY}}}\right) = 0. \tag{11}$$

Indeed from (11) these two conditions imply that $k_1 = k_2 = k_3 = k_4$ and consequently from (10) it implies that all four eigenvectors are identical. Substituting (4) into (11) and after some simplification, necessary and sufficient conditions to realize a fourth-order EPD at radian frequency ω_e in terms of the per-unit-length CTL parameters are obtained in their simplest form as

$$Z_1(\omega_e)Y_1^2(\omega_e) = -Z_2(\omega_e)Y_2^2(\omega_e) \tag{12}$$
$$Y_c(\omega_e) = \frac{-Y_1(\omega_e)Y_2(\omega_e)}{Y_1(\omega_e) + Y_2(\omega_e)}. \tag{13}$$

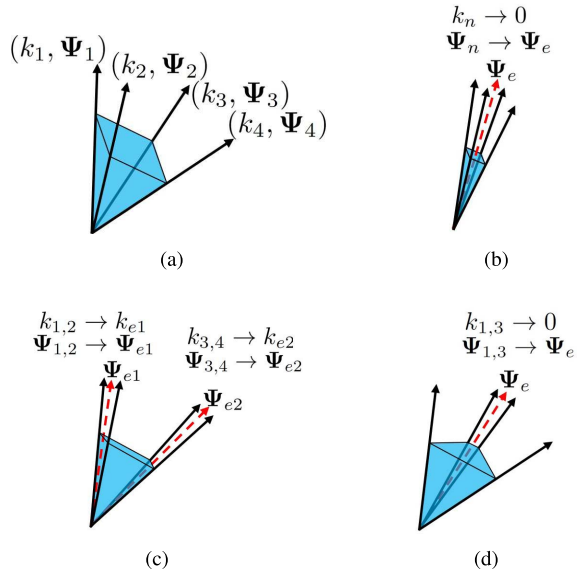

Fig. 3. Schematic representation of the four eigenvectors of the four eigenmodes supported by a CTL as they approach different EPDs conditions. (a) No EPD, i.e., the four eigenvectors are four independent vectors in a 4-D state space. (b) Fourth-order EPD, i.e., the four eigenvectors tend to coalesce into a single eigenstate. When the structure is lossless and gainless such fourth-order EPD is called DBE. (c) Two points of second-order degeneracy, i.e., pairs of eigenvectors coalesce to two independent eigenstates at the so called RBE. (d) Single second-order EPD, i.e., only two eigenvectors coalesce at the so-called RBE while the other two remain independent. The degree (i.e., the order) of degeneracy of a multimode EPD condition is given by the number of coalescing eigenvectors.

It is important to point out that the first condition in (12) represents a constraint on the parameters of the uncoupled TLs to have a DBE, whereas the second condition in (13) represents the constraint on the required coupling admittance to have a DBE. Therefore, just fixing the coupling parameter is not enough to have a DBE since the two individual TLs (without considering coupling) need to satisfy the constraint (12). Both terms $Y_1^2(\omega_e)$ and $Y_2^2(\omega_e)$ in (12) have a negative sign (we do not consider losses so far in this ideal analysis) regardless of the type of Y_1 and Y_2 susceptance. Consequently, from (12) and (13), we deduce that two necessary conditions to realize a fourth-order EPD at radian frequency ω_e for lossless and gainless CTLs are

$$\mathrm{Im}(Z_1)\mathrm{Im}(Z_2)\Big|_{\omega=\omega_e} < 0$$
$$\mathrm{Im}\left(Y_c^{-1}\right)\mathrm{Im}\left(Y_1^{-1} + Y_2^{-1}\right)\Big|_{\omega=\omega_e} < 0. \tag{14}$$

This means that the necessary condition to realize a DBE in uniform CTL is that the two series per-unit-length impedances Z_1 and Z_2 must be of different types, that is, one should be capacitive and the other inductive. Furthermore, Y_c^{-1} and $Y_1^{-1} + Y_2^{-1}$ must also be of different types. Fig. 4 shows all possible configurations of the per-unit-length parameters of CTLs that exhibit a fourth-order DBE.

From Fig. 4, it is concluded that a fourth-order DBE occurs in two uniform CTLs when there is a coupling between: a forward propagating mode and an evanescent mode [Fig. 4(a)],

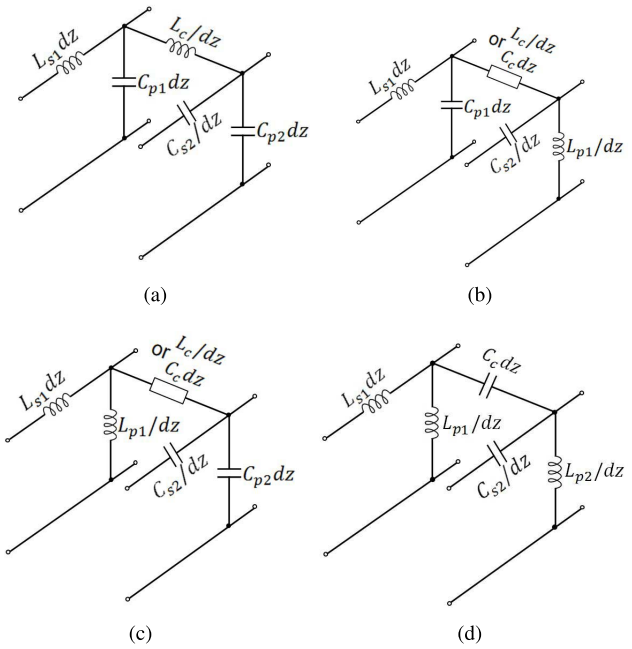

Fig. 4. Different configurations of uniform CTLs that may exhibit a fourth-order EPD, namely the DBE when the CTLs are lossless. Here, we show the combinations of distributed reactances that provide multimode degenerate conditions. Configuration (a) shows that a fourth-order EPD is obtained by a proper inductive coupling between a "forward" propagating mode in TL_1 and an evanescent mode in TL_2. Configuration (b) shows that a fourth-order EPD is obtainable by a proper coupling between a forward mode in TL_1 and a "backward" mode in TL_2. Note that here we denote a mode to be "forward" when phase and group velocities have the same signs, whereas a "backward" mode has phase and group velocities with opposite signs. Configuration (c) shows that a fourth-order EPD is obtainable also when proper coupling is designed between evanescent modes in TL_1 and TL_2. Finally, configuration (d) shows that an EPD can be obtained also by a capacitive coupling between an evanescent mode in TL_1 and a backward propagating mode in TL_2.

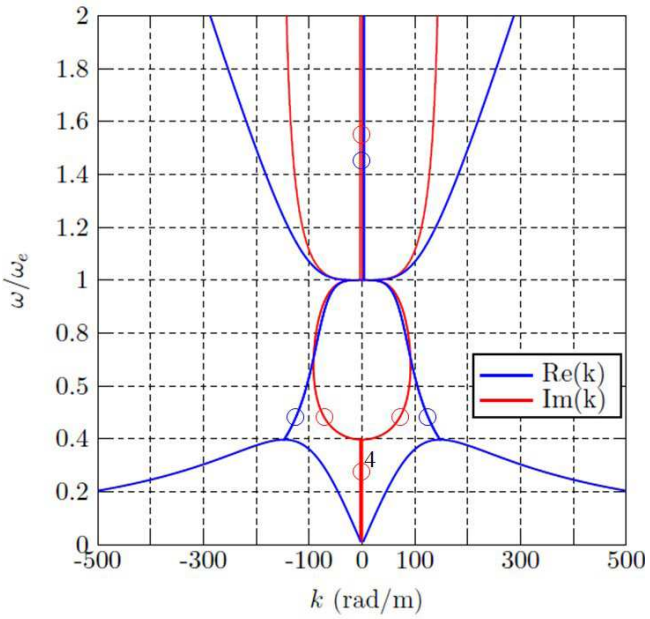

Fig. 5. Dispersion diagram of modal complex wavenumbers k versus normalized frequency for two uniform CTLs with distributed circuit model as in 4(a). The diagram shows a fourth-order DBE $\omega = \omega_e$, i.e., at $f = f_e = 5$ GHz, where all modes have $k = 0$. This CTL structure also exhibits two RBEs (EPDs of second order) at $\omega = 0.4\omega_e$, i.e., at $f = 2$ GHz, with a nonvanishing wavenumber of $k = \pm 147.5$ rad/m. Branches that represent two modes are denoted by a red or a blue circle, the branch representing four modes is tagged by red circles with number 4. The dispersion diagram showing *only* the purely real wavenumber branches is reported in Fig. 1(d).

forward and backward propagating modes [Fig. 4(b)], two evanescent modes [Fig. 4(c)], or a backward propagating mode and an evanescent mode [Fig. 4(d)]. For a rectangular waveguide structure, the configuration in Fig. 4(a) represents a coupling between a transverse electric (TE) or transverse magnetic (TM) propagating mode and a TM evanescent mode (below cutoff), whereas the configuration in Fig. 4(c) represents coupling between TE and TM evanescent modes, both below cutoff when considered without coupling [30].

A. Example of Uniform CTL With Infinite Length

Two CTLs with circuit configuration as in Fig. 4(a) are designed to exhibit a fourth-order EPD at frequency $f_e = 5$ GHz, i.e., to satisfy the DBE conditions in (12) and (13). The CTLs parameters are $C_{p1} = C_{p2} = 0.12$ nF/m, $L_{s1} = 200$ nH/m, $C_{s2} = 5.07$ fFm and $L_c = 16.89$ pHm, where the series and parallel per-unit-length components are designated with subscripts s and p, respectively. This is the case when one TL (without considering the coupling between the two TLs) supports two propagating modes (one in each direction) while the other TL supports evanescent waves. However, the two TLs are coupled via the inductive subsceptance $Y_c = 1/(j\omega L_c)$ leading to the modal dispersion diagram in Fig. 5. There, both the real and imaginary parts of the wavenumber are shown versus real radian frequency. A fourth-order DBE occurs at radian frequency $\omega_e = 31.42 \times 10^9$ rad/s at which $k_1 = k_2 = k_3 = k_4 = 0$. Note that the dispersion diagram also exhibits two second-order EPDs which represent two RBEs at $\omega = 0.4\omega_e$ (i.e., at $f \approx 2$ GHz) at two distinct nonvanishing wavenumbers $k = \pm 147.5$ rad/m, where their sufficient condition $T^2 = 4D$ is satisfied at this particular frequency. In the bandgap $0.4\omega_e < \omega < \omega_e$ the diagram has four wavenumbers with complex values that describe exponential decay. For $\omega > \omega_e$ two waves are propagating (purely real k) and two are evanescent (purely imaginary k). The same dispersion diagram showing *only* the branches with purely real wavenumbers is reported in Fig. 1(d). Therefore, the CTL technique used in this article allows to put regular band edges at properly designed wavenumbers.

B. Uniform Waveguide With Finite Length

So far we have discussed modal propagation in infinitely long structures. We now consider two uniform CTLs with finite length L, Fig. 6(a), operating in very close proximity of the DBE, and investigate the transmission properties in terms of scattering parameter $|S_{21}|$. Since this finite length CTL structure forms a resonator, we also investigate its quality factor. The CTL per-unit-length parameters are the same as those used in Section III-A that led to Fig. 5. There are two ports, at the beginning and end of TL_1, whereas TL_2 is terminated on short circuits at both ends, as depicted in Fig. 6(a). Fig. 6(b) shows the transmission coefficient magnitude $|S_{21}|$ versus frequency, for different lengths L.

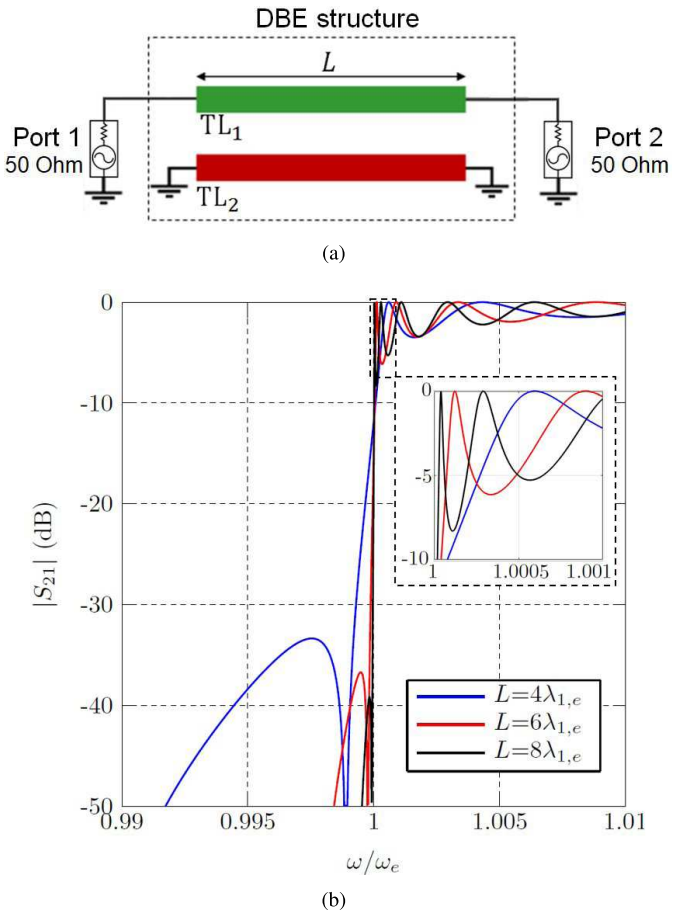

Fig. 6. Magnitude of the transmission scattering parameter S_{21} for the waveguide consisting of two uniform microstrip CTLs with finite length L, with distributed circuit model as in 4(a). The CTLs have a fourth-order EPD (namely, a DBE) at the so-called DBE frequency $f = f_e = 5$ GHz. (a) Finite length CTL circuit setup. (b) Scattering parameter S_{21} for different lengths L revealing that this finite length CTL structure is a cavity despite the characteristic impedance of TL_1 is equal to the termination load. A clear transmission peak, called DBE resonance, is observed near the DBE frequency, and it gets narrower for increasing lengths. $\lambda_{1,e}$ is the wavelength of the propagating waves in TL_1, when it is uncoupled to TL_2, calculated at the EPD frequency $\lambda_{1,e} = 2\pi/k_{1,e} = 40.8$ mm, where $k_{1,e} = \omega_e(L_{s1}C_{p1})^{1/2}$.

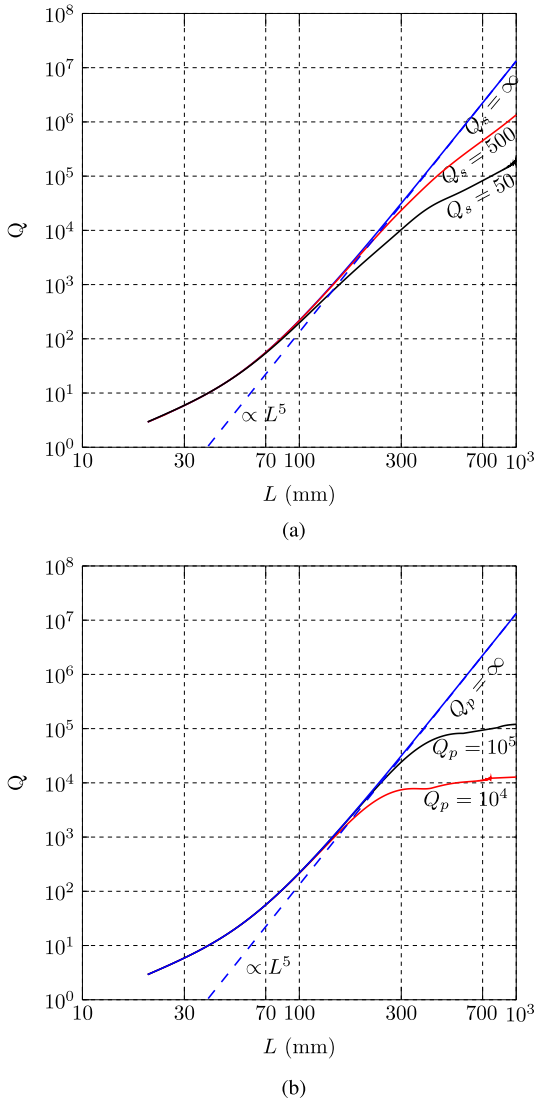

Fig. 7. Trend of the quality factor of a CTL cavity as in Fig. 6(a) operating at the DBE resonance, in close proxinity of the DBE frequency, showing the L^5 scaling with cavity length L. When the CTL cavity has distributed losses, the quality factor trend is perturbed. Distributed series resistance and parallel conductance are assumed to be symmetrical, i.e., identical in each TL. (a) Series losses only. (b) Parallel losses only. The legend $Q = \infty$ refers to the limit represented by a lossless CTL cavity and the blue dashed line is a fitting trend showing the L^5 growth with cavity length. These plots show that the Q factor of the CTL cavity is less sensitive to series losses.

The length is here given in terms of wavelengths of the propagating wave in TL_1, when uncoupled to TL_2, calculated at the EPD frequency $\lambda_{1,e} = 2\pi/k_{1,e} = 40.8$ mm, where $k_{1,e} = \omega_e(L_{s1}C_{p1})^{1/2}$. The passband property is in agreement with that shown in Fig. 5, i.e., there is propagation for $f > f_e = 5$ GHz. It is shown that the CTL exhibits a resonance (called DBE resonance) at a frequency almost coincident with the DBE one, regardless of the CTL length, at least for the two longer cases. The frequency of the other resonances at lower frequencies are strongly affected by the length of the structure. This resonator based on a multimode degeneracy exhibits a very interesting physical behavior of its quality factor. The loaded quality factor of the finite length and lossless CTL is plotted versus length L in Fig. 7, and it is concluded that such quality factor (blue line) follows the asymptotic trend proportional to L^5 as L increases, which is the same conclusion that was made in [4], [5], [15], and [31], though in these references the DBE was obtained in periodic structures and at the edge of the Brillouin zone, whereas in this article we show for the first time a DBE at $k = 0$. Here, the quality factor has been evaluated as $Q = \omega_{\text{res}}\tau_g/2$, where ω_{res} is the resonance frequency associated with maximum transmission, that is, where $|S_{21}|$ is maximum, and the group delay τ_g is calculated as the derivative of the phase of S_{21}, with respect to the angular frequency ω, that is, $\tau_g = \partial(\angle S_{21})/\partial\omega$ [32]. Note that high Q values are obtained while the TL_1 characteristic impedance (without considering the coupling) is 50 Ω and the termination load is also 50 Ω; therefore TLs forming a cavity using the four mode degenerate condition (the DBE) do not need high reflection coefficients at the end of each TL. The strong reflection of the degenerate modes at the end of the CTL occurs because the characteristic impedance of a CTL made of two TLs is actually represented by a 2×2 impedance matrix,

and therefore it is generally mismatched when two independent loads are used as termination as in Fig. 6(a). Furthermore, exactly at the DBE frequency the group velocities of the four coalescing modes vanish and therefore the characteristic 2×2 matrix impedance shall describe the absence of power flow (the characteristic impedance of a *single* TL at cutoff would be either zero or infinity). However, one should note that the DBE *resonance* is slightly shifted from the DBE frequency and therefore power transfer to the load is actually occurring. It is important to point out that there are various resonance frequencies in the cavity, however, in this article, we are focusing on the nearest one to the DBE frequency which we call it the first resonance frequency. Because of the DBE-like dispersion relation in (2), for long cavities the first DBE resonance frequency is approximated by the asymptotic formula

$$f_{\text{res},1} = f_e + \alpha/L^4 \tag{15}$$

where α is a constant. This implies that the longer the CTL cavity, the closer the DBE resonance is to the DBE frequency, and hence the less power leakage occurs outside the resonator.

A further investigation is now conducted by studying the effect of series and parallel distributed losses in the CTL on the quality factor. Therefore, we assume that each TL has either a per-unit-length series resistance R_s or a per-unit-length shunt conductance G_p. Accordingly, Fig. 7(a) plot the quality factor of the CTL versus length L for different values of the series quality factor Q_s, where $Q_s = \omega_e L_{s1}/R_s = 1/(\omega_e C_{s2} R_s)$ is the quality factor (assumed the same) of the two series elements, which are an inductive distributed reactance in TL_1 and a capacitive distributed reactance in TL_2, and hence they satisfy $\omega_e L_{s1} = 1/(\omega_e C_{s2})$. In Fig. 7(b) instead we show the quality factor by considering losses in the two shunt (parallel) capacitive susceptances such that $Q_p = \omega C_{p1}/G_{p1} = \omega C_{p2}/G_{p2}$. Note that the same parallel capacitor and the same loss is used in each of the two TLs. The two plots show a very important fact about *uniform* CTLs exhibiting a fourth-order DBE: the quality factor of the CTLs is robust to the series losses, that is, the series distributed resistance does not affect the total quality factor trend shown in Fig. 7(a). This occurs because the wavenumbers of the four modes at DBE are such that $k_1 = k_2 = k_3 = k_4 = 0$, which means the voltage along the finite length CTL is basically constant resulting in an almost vanishing current through the series elements Z_1 and Z_2. However, when losses are in the shunt (parallel) elements the quality factor of the structure tends to saturate to the quality factor of the used distributed parallel capacitors as shown in Fig. 7(b). To obtain such plots, for each CTL length we have determined the resonant frequency and evaluated the required parameters at that frequency.

It is important to point out that the resonance mentioned in the previous study is not a conventional resonance due to two mode reflection, however, it is due to four modes which make it with very unique properties like quality factor and resonance frequency scaling with cavity length. Such properties can be used to make an oscillator with a unique mode selection scheme that leads to a stable single-frequency oscillation, even in the presence of load variation [21], [33]. Moreover, the proposed DBE in this article exists at $k = 0$ which make good candidate for application like leaky wave antennas, and active leaky wave antennas that act as radiating oscillators.

IV. Microstrip Implementation With Subwavelength Series Capacitors

A microstrip implementation of the uniform CTL in Fig. 4(a) is now considered where the series continuously distributed capacitance is approximated by a periodic capacitive loading with subwavelength period $d = \lambda_d/10$, where λ_d is wavelength in the substrate. Furthermore, the guided wavelength $\lambda_g = 2\pi/k$ in the proximity of the DBE at $k = 0$ is very large, and tends to infinity when k tends to zero. Therefore, because of the very subwavelength period $d \ll \lambda_g$, the CTL can be seen as a homogenized medium according to metamaterial homogenization concepts [34], [35]. Indeed we design the CTL such that the homogenized effective CTL parameters approximately equal those in the uniform case considered in Section III. The grounded dielectric substrate has a relative dielectric constant of 2.2, loss tangent 0.001, and height of 0.75 mm. Metal layers have a conductivity of 4.5×10^7 S/m and thickness of 35 μm. The series capacitance in each unit cell is implemented using an interdigital capacitor and the coupling inductance in Fig. 4(a) is implemented using a folded short and thin microstrip between the two TLs as shown in Fig. 8. The two TL widths (i.e., when assumed uncoupled, and before introducing the series capacitors) are designed to have a characteristic impedance of 50 Ω at $f = 5$ GHz. All the dimensions (in mm) are reported in Fig. 8. The interdigital capacitance is approximately $C_d = 1$ pF, and since the period is $d = 5.1$ mm, then the effective distributed series capacitance is the same as the required one to get DBE, that is, $C_{s1} = C_d d \approx 5.1$ fFm.

Fig. 9(a) shows the modal dispersion obtained using full wave simulations based on the method of moments implemented in Keysight Technologies Advanced Design System (ADS). The used method of moments is based on the 3-D Green's function with all the dynamic terms, hence including radiation losses. The dispersion relation was calculated by determining the S-parameters of a single unit-cell, then converting them to a 4×4 unit-cell transfer matrix $\mathbf{T}_U$ that relates voltages and currents at the beginning and end of the unit cell as in [18], and then using the Floquet theorem determining the eigenvalue problem that provides the four modal wavenumbers (see also Appendix A). Fig. 9(a) shows the existence of a DBE in the dispersion diagram, and in proximity of ω_e it is in good agreement with the diagram of the uniform ideal CTL in Fig. 5.

We then observe the quality factor of a resonator made by a finite-length dual microstrip, shown in Fig. 8. The loading and excitation for calculating the quality factor are as shown in Fig. 6(a), and the operating frequency is at the DBE resonance (the peak of the transfer function closest to the DBE frequency). The quality factor is estimated by the same formula considered in Section III, that is, by $Q = \omega_{\text{res}} \tau_g/2$, where the resonance frequency (the one closest to the DBE frequency) depends on the cavity length.

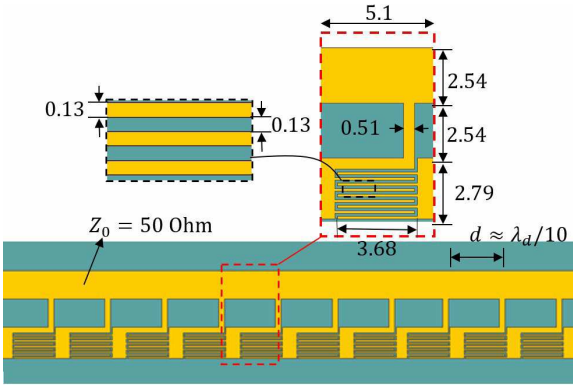

Fig. 8. Microstrip implementation of two uniform CTLs over a grounded dielectric substrate, with circuit model as in Fig. 4(a), i.e., with a distributed series capacitor (bottom line) that is here implemented by resorting to a periodic distribution of series interdigital capacitors, with subwavelength period d. The bottom part of the figure shows the finite length CTLs, whereas the top part of the figure shows the unit cell with period $d = 5.1$ mm. Dimensions are all in mm. This microstrip CTL implementation develops a fourth-order EPD at $f = f_e = 5$ GHz.

The quality factor versus "cavity" length $L = Nd$, using N unit cells of the microstrip implementation in Fig. 8, is plotted in Fig. 9. From this figure, we note that the quality factor tends to saturate before exhibiting the asymptotic L^5 trend because of radiation, conduction and dielectric losses. Indeed the ideal $Q \propto L^5$ trend depicted in Fig. 7 (blue line) occurs only in the ideal case where losses are negligible, whereas in this case both series and shunt losses are present because of copper and dielectric losses. Note that here the TL_1 characteristic impedance is 50 Ω and that the load is also 50 Ω, therefore a cavity using the four mode degenerate condition (the DBE) does not need high reflection coefficients at the end of each TL that can be normally terminated at any load.

V. Experimental Verification Using a CTL With Discrete Series Capacitor

In this section, we show an experimental verification of the existence of the DBE when evanescent modes are coupled in the CTL. Fig. 10 shows the microstrip implementation of the uniform CTL in Fig. 4(a). The unit-cell is fabricated on a grounded dielectric substrate (Rogers substrate RT/duroid 5880) with a relative dielectric constant of 2.2, loss tangent of 0.001, and height of 0.79 mm. We use here discrete component capacitors to periodically load one TL to support evanescent modes. We use surface mount ceramic capacitors (manufactured by Murata Electronics, part number GJM1555C1H3R1BB01D) with a capacitance of 3.1 pF and quality factor of $Q > 50$ for $f < 3$ GHz. All the TLs have a width of $w = 2.4$ mm to have a characteristic impedance of 50 Ω. The structure has period of $d = 10.5$ mm ($d \sim \lambda_d/10$) and stubs length $\ell = 19$ mm. As discussed in Section III, the CTL can be seen as uniform, due to the subwavelength period.

To confirm the existence of EPDs in the periodic CTL, we analyze a unit-cell and perform scattering (S)-parameter measurements using a four-port Rohde & Schwarz vector network analyzer (VNA) ZVA 67. Fig. 11(a) shows the fabricated

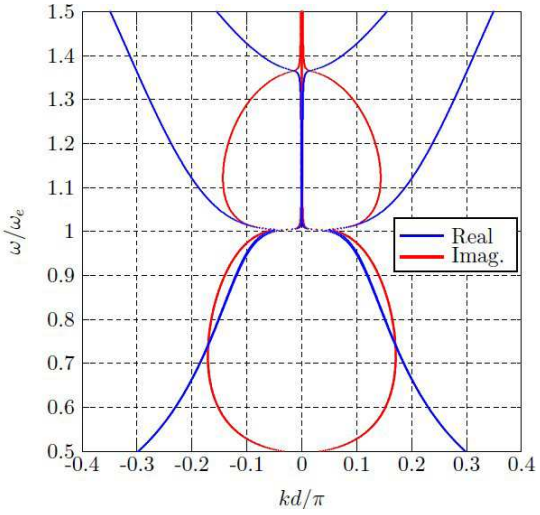

(a)

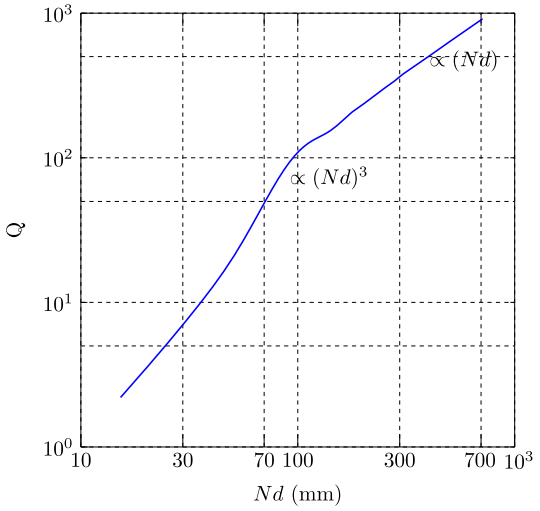

(b)

Fig. 9. Results relative to the microstrip implementation of the uniform CTLs using a periodic distribution of interdigital series capacitors in TL_2, with subwavelength period (Fig. 8). (a) Dispersion diagram obtained via full-wave simulation showing the complex modal wavenumbers versus frequency. The full-wave simulation reveals the existence of a DBE (a fourth-order degeneracy) at $k = 0$. The simulation accounts for radiation, dielectric and copper losses. (b) Quality factor of the periodic CTLs versus resonant "cavity" length, showing its scaling with the number of unit cells N.

unit-cell with 5-mm extension on both sides to be able to solder the SMA connectors. The measured scattering matrix is then transformed into a 4×4 transfer matrix $\underline{\mathbf{T}}_A$. However, this transfer matrix, of the microstip in Fig. 11(a) that includes extensions, is not the same as the transfer matrix of the one unit cell $\underline{\mathbf{T}}_U$, however, it is a cascaded version of it. The total transfer matrix is $\underline{\mathbf{T}}_A = \underline{\mathbf{T}}_R \underline{\mathbf{T}}_U \underline{\mathbf{T}}_L$, where $\underline{\mathbf{T}}_R$ and $\underline{\mathbf{T}}_L$ account for the extra lengths constituting the extensions at both sides and the SMA connectors. In Fig. 11(b), we show the microstrip used in the two extensions, connected as a "through", for calibration purposes. The transfer matrix of the two connected extensions is $\underline{\mathbf{T}}_B = \underline{\mathbf{T}}_R \underline{\mathbf{T}}_L$. Now a matrix that is proportional to the unit-cell transfer matrix $\underline{\mathbf{T}}'_U$ is obtained by deembedding $\underline{\mathbf{T}}_B$ from $\underline{\mathbf{T}}_A$, that is, $\underline{\mathbf{T}}'_U = \underline{\mathbf{T}}_A \underline{\mathbf{T}}_B^{-1} = \underline{\mathbf{T}}_R \underline{\mathbf{T}}_U \underline{\mathbf{T}}_R^{-1}$. It is

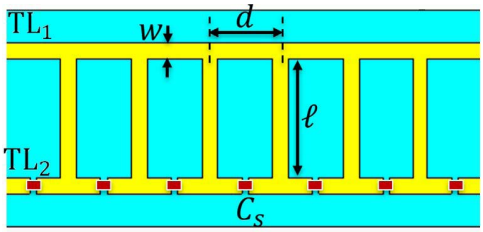

Fig. 10. Microstrip implementation of a waveguide made of two coupled uniform TLs over a grounded dielectric substrate in Fig. 4(a) that exhibits DBE. TL_1 (when uncoupled from TL_2) supports propagation. Whereas TL_2 (when uncoupled from TL_1) supports evanescent modes because it is loaded with distributed series capacitors mimicking a uniform series capacitive per-unit-length distribution. The capacitors in this structure are discrete components with value 3.1 pF. The inductive coupling between the two TLs is implemented using stubs connected between the transmission lines TL_1 and TL_2. The period is small compared to the guided wavelength.

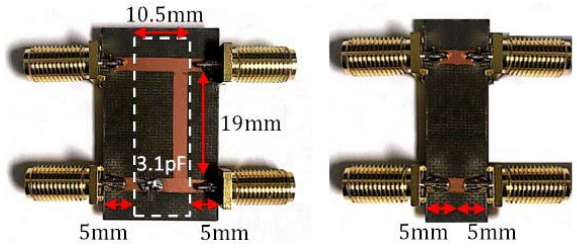

(a) (b)

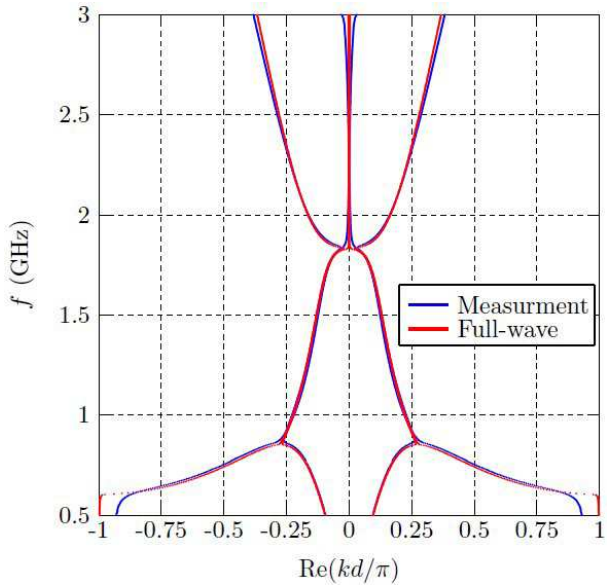

(c)

Fig. 11. (a) Fabricated unit-cell for the CTL in Fig. 10 with 5-mm extensions on both sides to be able to solder the SMA connectors. (b) Fabricated microstrip extensions used for calibration, that is, to deembed the effect of the extra extensions and SMA connectors from (a). (c) Wavenumber dispersion versus frequency showing the existence of the DBE around 1.85 GHz, and two second-order EPDs (i.e., RBE) around 0.86 GHz. The measured result is in very good agreement with that from full-wave simulations.

important to point out that although $\underline{\mathbf{T}}_U$ and $\underline{\mathbf{T}}'_U$ are not identical but they share the same eigenvalues because $\underline{\mathbf{T}}'_U$ is just a transformed version of $\underline{\mathbf{T}}_U$. An analogous procedure based on comparing transfer matrices of CTLs with 8 and 9 unit cells was adopted in [36]. Using Floquet theory, following [18], the dispersion relation of the four modes is obtained

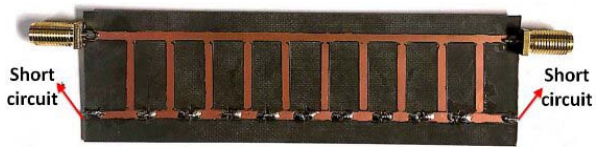

(a)

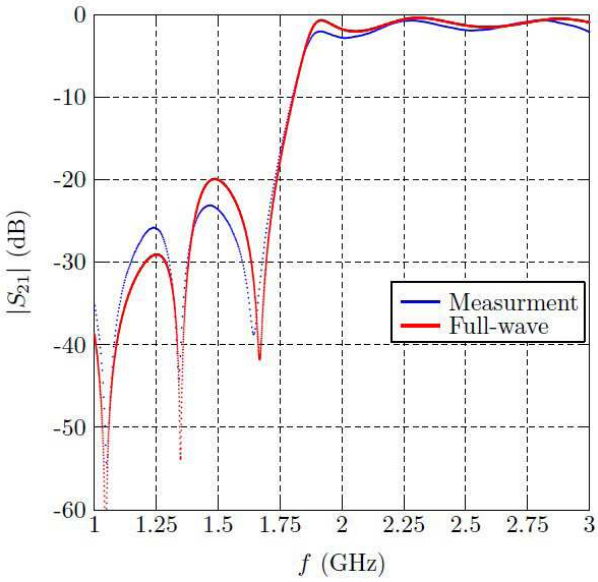

(b)

Fig. 12. Measurements and simulations of the scattering parameter S_{21} for a nine-unit-cell CTL in (a). The result is consistent with the DBE observation in the dispersion diagram at $f = 1.85$ GHz. The good agreement between full-wave simulations and measurements shows that there is a DBE resonance associated with the DBE.

as: $e^{jkd} = \text{eig}(\underline{\mathbf{T}}_U)$ (i.e., the four eigenvalues of $\underline{\mathbf{T}}_U$) and since $\underline{\mathbf{T}}_U$ and $\underline{\mathbf{T}}'_U$ have identical eigenvalues, the dispersion is determined finally in the form of $e^{jkd} = \text{eig}(\underline{\mathbf{T}}'_U) = \text{eig}(\underline{\mathbf{T}}_A \underline{\mathbf{T}}_B^{-1})$, where $\underline{\mathbf{T}}_A$ and $\underline{\mathbf{T}}_B$ are the transfer matrices for the two four-port microstips in Fig. 11(a) and (b), respectively. The wavenumber dispersion diagram in Fig. 11(c) shows the four coalescing complex wavenumbers (only the real parts are shown for brevity, the imaginary parts is analogous to that in Fig. 5). In summary, the wavenumber dispersion diagram based on measurements is in good agreement with the results based on the S-parameters calculated via full-wave simulations based on the finite element method implemented in CST Studio Suite. The dispersion shows several frequencies at which EPD exists: a fourth-order EPD (the DBE) at $f \approx 1.85$ GHz and two second-order EPDs (the RBEs) at $f \approx 0.86$ GHz. The perturbation due to ohmic, dielectric, and radiation losses seems negligible because it does not destroy the occurrence of the EPDs.

Fig. 11(c) shows a nine-unit-cell of the same DBE structure. The lower TL is connected to two short circuits, similar to the setup shown in Fig. 6(a). We show in Fig. 12(b) the measurement and full-wave simulation based on the finite element method, of the magnitude of the scattering parameter S_{21}. These results show good agreement between simulation and measurement. The results also demonstrate the occurrence of the DBE resonance at 1.9 GHz that is close to the DBE frequency of 1.85 GHz.

VI. Conclusion

We have shown the general conditions demonstrating that a fourth-order EPD, namely a DBE, occurs at $k = 0$ in two *uniform* lossless and gainless CTLs when there is proper coupling between: 1) propagating modes and evanescent modes, 2) forward and backward propagating modes, or 3) four evanescent modes. We show that the resonance frequency of a cavity made of a finite-length CTLs exhibiting a DBE is very close to the DBE frequency, moreover, we show that the quality factor increases with the fifth power of the cavity length (in the lossless case) and such trend is robust to the occurrence of series losses. Furthermore, we have shown that by using the CTL concept, a *RBEs* can be designed at nonvanishing wavenumbers. An example of CTLs supporting the EPD wave phenomena discussed in this article has been presented using a metamaterial-based CTLs where the period to realize series capacitances is subwavelength. We have provided the experimental demonstration of the occurrence of the DBE in two uniform CTLs using a metamaterial-like periodic CTL with subwavelength period, implemented in microstrips. Possible applications exploiting the physics of the DBE and the RBE are in high quality factor cavities [5], radio frequency oscillators [21] and distributed oscillators [33], leaky wave antennas [9], filters, pulse compression [14], sensors, high power electron-beam devices [20], and lasers [22].

Appendix A
General Solution of Wave Equation of Two Uniform Coupled Waveguides

Considering two coupled uniform TLs, the telegrapher's equations that describe wave propagation are described by a first-order differential equation in (6). The general solution of (6) with an initial condition Ψ_{zo} at $z = 0$ is given by

$$\Psi(z) = \exp\left(-j\underline{\mathbf{M}}z\right)\Psi_{zo}. \tag{16}$$

The matrix $\exp(-j\underline{\mathbf{M}}z)$ is called transfer matrix. The system matrix $\underline{\mathbf{M}}$ is diagonalizable when it has distinct eigenvectors, and the eigenvalues k_1, k_2, k_3, and k_4, and the eigenvectors Ψ_1, Ψ_2, Ψ_3, and Ψ_4, of $\underline{\mathbf{M}}$ are determined by solving the eigenvalue problem $\underline{\mathbf{M}}\Psi = k\Psi$. The matrix $\exp(-j\underline{\mathbf{M}}z)$ in (16) is generally determined by diagonalizing the matrix $\underline{\mathbf{M}}$, however, at EPDs where some of the eigenvectors coalesce, the system matrix $\underline{\mathbf{M}}$ cannot be diagonalized and indeed the matrix $\underline{\mathbf{M}}$ is similar to a matrix that contains at least a nontrivial Jordan block [1], [3].

A. Diagonalizable System Matrix

When $\underline{\mathbf{M}}$ has distinct eigenvectors, That is, none of the eigenmode coalesce, it can be diagonalized and represented as

$$\underline{\mathbf{M}} = \underline{\mathbf{U}}\ \underline{\Lambda}\ \underline{\mathbf{U}}^{-1} \tag{17}$$

where $\underline{\mathbf{U}}$ is the similarity transformation matrix containing all the eigenvectors of $\underline{\mathbf{M}}$ as columns and it is written in the form $\underline{\mathbf{U}} = [\Psi_1|\Psi_2|\Psi_3|\Psi_4]$, whereas the matrix $\underline{\Lambda}$ is a diagonal matrix containing all the eigenvalues of $\underline{\mathbf{M}}$, viz., $\Lambda_{nn} = k_n$ for $n = 1, 2, 3, 4$. Since the eigenvectors of the system are distinct, they form a complete set to represent any state vector at any coordinate z. As a consequence, the initial condition Ψ_{zo} can be represented as a linear decomposition of the eigenvectors (See Ch. 4 in [37]) as

$$\Psi_{zo} = a_1\Psi_1 + a_2\Psi_2 + a_3\Psi_3 + a_4\Psi_4 = \underline{\mathbf{U}}\ \mathbf{a} \tag{18}$$

where a_n are the weights of each eigenvector, and the vector $\mathbf{a}$ is written in the form $\mathbf{a} = [\,a_1\ \ a_2\ \ a_3\ \ a_4\,]^{\mathrm{T}}$.

Substituting (17) and (18) in (16) yields

$$\begin{aligned}\Psi(z) &= \underline{\mathbf{U}}\exp\left(-j\underline{\Lambda}z\right)\underline{\mathbf{U}}^{-1}\Psi_{zo}\\ &= \underline{\mathbf{U}}\exp\left(-j\underline{\Lambda}z\right)\mathbf{a}\\ &= \left[\Psi_1 e^{-jk_1z}|\Psi_2 e^{-jk_2z}|\Psi_3 e^{-jk_3z}|\Psi_4 e^{-jk_4z}\right]\mathbf{a}\\ &= a_1\Psi_1 e^{-jk_1z} + a_2\Psi_2 e^{-jk_2z}\\ &\quad + a_3\Psi_3 e^{-jk_3z} + a_4\Psi_4 e^{-jk_4z}.\end{aligned} \tag{19}$$

From (19), it is clear that the general solution of the wave equation is decomposed of four eigenmodes, where each mode separately is varying as $\Psi \propto e^{-jk_nz}$.

B. Nondiagonalizable System Matrix With Fourth-Order EPD

At a fourth-order EPD, the eigenvalues and the eigenvectors of $\underline{\mathbf{M}}$ coalesce, so $k_n = k_e$ and $\Psi_n = \Psi_e$ for $n = 1, 2, 3, 4$, where k_e and Ψ_e are the degenerate eigenvalue and eigenvector, respectively. The system matrix $\underline{\mathbf{M}}$ is not diagonalizable, whereas, the matrix $\mathbf{U}$ constructed as described in Appendix A-A at any frequency near the EPD will be singular exactly at the EPD (as a limit process). Hence the non-diagonizable $\mathbf{M}$ is similar to a matrix in Jordan normal form (See Ch. 7 in [37]) as

$$\underline{\mathbf{M}} = \underline{\mathbf{W}}\ \left(k_e\underline{\mathbf{1}} + \underline{\mathbf{N}}\right)\ \underline{\mathbf{W}}^{-1} = k_e\underline{\mathbf{1}} + \underline{\mathbf{W}}\ \underline{\mathbf{N}}\ \underline{\mathbf{W}}^{-1} \tag{20}$$

where $\underline{\mathbf{1}}$ is a 4×4 identity matrix, and $\underline{\mathbf{N}}$ is a Nilpotent matrix

$$\underline{\mathbf{N}} = \begin{pmatrix}0 & 1 & 0 & 0\\ 0 & 0 & 1 & 0\\ 0 & 0 & 0 & 1\\ 0 & 0 & 0 & 0\end{pmatrix} \tag{21}$$

and it follows the property:

$$\mathbf{N}^n = \mathbf{0}\quad \forall\ n \geq 4. \tag{22}$$

The matrix $\underline{\mathbf{W}}$ contains the *generalized* eigenvectors of $\underline{\mathbf{M}}$ and is written in the form $\underline{\mathbf{W}} = [\Psi_e|\Psi_{e1}|\Psi_{e2}|\Psi_{e3}]$, where

$$\begin{aligned}\underline{\mathbf{M}}\Psi_e &= \mathbf{0},\\ \underline{\mathbf{M}}\Psi_{e1} &= \Psi_e\\ \underline{\mathbf{M}}\Psi_{e2} &= \Psi_{e1}\\ \underline{\mathbf{M}}\Psi_{e3} &= \Psi_{e2}.\end{aligned} \tag{23}$$

Substituting (20) in (16) gives

$$\Psi(z) = \exp\left(-jk_ez\underline{\mathbf{1}} - jz\underline{\mathbf{W}}\ \underline{\mathbf{N}}\ \underline{\mathbf{W}}^{-1}\right)\Psi_{zo}. \tag{24}$$

Since the matrix $k_e\underline{\mathbf{1}}$ and $\underline{\mathbf{W}}\ \underline{\mathbf{N}}\ \underline{\mathbf{W}}^{-1}$ commute (See Ch. 10 in [38]), then (24) is simplified to

$$\Psi(z) = e^{-jk_e z}\exp\left(-jz\underline{\mathbf{W}}\ \underline{\mathbf{N}}\ \underline{\mathbf{W}}^{-1}\right)\Psi_{zo}. \tag{25}$$

Using the Taylor series expansion of the exponential function (See Ch. 10 in [38]) and using the fact that $(\underline{\mathbf{W}}\ \underline{\mathbf{N}}\ \underline{\mathbf{W}}^{-1})^n = \underline{\mathbf{W}}\ \underline{\mathbf{N}}^n\ \underline{\mathbf{W}}^{-1}$ for any integer n, (25) is expanded as

$$\Psi(z) = e^{-jk_e z}\sum_{n=0}^{\infty}\frac{\underline{\mathbf{W}}(-\mathbf{jz}\underline{\mathbf{N}})^{\mathbf{n}}\ \underline{\mathbf{W}}^{-\mathbf{1}}}{n!}\Psi_{zo} \tag{26}$$

and making use of (22), (26) is reduced to

$$\Psi(z) = e^{-jk_e z}\underline{\mathbf{W}}\left(\underline{\mathbf{1}} - jz\underline{\mathbf{N}} - \frac{z^2\underline{\mathbf{N}}^2}{2} + \frac{jz^3\underline{\mathbf{N}}^3}{6}\right)\underline{\mathbf{W}}^{-1}\Psi_{zo}. \tag{27}$$

At a fourth-order EPD the state vector Ψ_{zo} at $z = 0$ is represented as a series combination of the generalized eigenvectors as

$$\Psi_{zo} = a_e\Psi_e + a_{e1}\Psi_{e1} + a_{e2}\Psi_{e2} + a_{e3}\Psi_3 = \underline{\mathbf{W}}\ \mathbf{a}_e \tag{28}$$

where a_{en} are the weights of the generalized eigenvectors, and the vector $\mathbf{a}_e$ is written in the form $\mathbf{a}_e = [\,a_e\ \ a_{e1}\ \ a_{e3}\ \ a_{e3}\,]^{\mathrm{T}}$.

Substituting (28) into (26), the general solution at fourth-order EPD is obtained as

$$\begin{aligned}\Psi_{\mathrm{e}}(z) &= e^{-jk_e z}\underline{\mathbf{W}}\left(\underline{\mathbf{1}} - jz\underline{\mathbf{N}} - \frac{z^2\underline{\mathbf{N}}^2}{2} + \frac{jz^3\underline{\mathbf{N}}^3}{6}\right)\mathbf{a}_e\\ &= e^{-jk_e z}\underline{\mathbf{W}}\left[\,a_e,\quad a_{e1},\quad a_{e2},\quad a_{e3}\,\right]^{\mathrm{T}}\\ &\quad -, jze^{-jk_e z}\underline{\mathbf{W}}\left[\,a_{e1},\quad a_{e2},\quad a_{e3},\quad 0\,\right]^{\mathrm{T}}\\ &\quad -, \frac{z^2}{2}e^{-jk_e z}\underline{\mathbf{W}}\left[\,a_{e2},\quad a_{e3},\quad 0,\quad 0\,\right]^{\mathrm{T}}\\ &\quad -, jz^3e^{-jk_e z}\underline{\mathbf{W}}\left[\,a_{e3},\quad 0,\quad 0,\quad 0\,\right]^{\mathrm{T}}.\end{aligned} \tag{29}$$

Simplifying (29), the general solution of (6) is cast in the form

$$\begin{aligned}\Psi_{\mathrm{e}}(z) &= a_e\Psi_e e^{-jk_e z}\\ &\quad + a_{e1}(\Psi_{e1} - jz\Psi_e)e^{-jk_e z}\\ &\quad + a_{e2}\left(\Psi_{e2} - jz\Psi_{e1} - \frac{z^2}{2}\Psi_e\right)e^{-jk_e z}\\ &\quad + a_{e3}\left(\Psi_{e3} - jz\Psi_{e2} - \frac{z^2}{2}\Psi_{e1} + j\frac{z^3}{6}\Psi_e\right)e^{-jk_e z}.\end{aligned} \tag{30}$$

From (30), we conclude that only one mode preserve the proportionality $\Psi \propto e^{-jkz}$ at the fourth order EPD, while the other three modes have algebraic growth with z as $\Psi \propto \mathbf{P}(z)e^{-jkz}$, where $\mathbf{P}(z)$ is a polynomial vector function of maximum order of 3.

For waveguides where the two equivalent CTLs are described by the per-unit length parameters model as in Fig. 1(c) the generalized eigenvectors in (30) are explicitly found to be

$$\begin{aligned}\Psi_e &= \left[\,1,\quad -Y_1/Y_2,\quad 0,\quad 0\,\right]^{\mathrm{T}}\\ \Psi_{e1} &= \left[\,0,\quad 0,\quad j/Z_1,\quad jY_2/(Y_1Z_1)\,\right]^{\mathrm{T}}\\ \Psi_{e2} &= \left[\,-(Y_1+Y_2)/\left(Y_1^2Z_1\right),\quad 0,\quad 0,\quad 0\,\right]^{\mathrm{T}}\\ \Psi_{e2} &= \left[\,0,\quad 0,\quad -j(Y_1+Y_2)/\left(Y_1^2Z_1^2\right),\quad 0\,\right]^{\mathrm{T}}.\end{aligned} \tag{31}$$

Appendix B
Solution of Eigenvalue Problem for Uniform Coupled Waveguides

Consider two *uniform* CTLs described by generic per-unit-length distributed parameters as shown in Fig. 1(c). In this appendix, we follow the derivation in [28] to determine the wavenumbers of two *uniform* CTLs. The wave propagation in the structure is described by the first-order differential equations in (3). The wave equation describing wave propagation in the two CTLs is obtained by taking the derivative of the first equation in (3) with respect to z, and by inserting it into the second equation of (3), leading to

$$\frac{d^2\mathbf{V}(z)}{dz^2} = \underline{\underline{\mathbf{Z}}}(\omega)\ \underline{\underline{\mathbf{Y}}}(\omega)\mathbf{V}(z). \tag{32}$$

The assumption of having propagating waves with function along the z-direction $\mathbf{V}(z) \propto e^{-jkz}$ makes the possible solutions of (32) cast in an eigenvalue problem form

$$k^2\mathbf{V}(z) = -\underline{\underline{\mathbf{Z}}}(\omega)\ \underline{\underline{\mathbf{Y}}}(\omega)\mathbf{V}(z). \tag{33}$$

Although the matrix $\underline{\underline{\mathbf{Z}}}\ \underline{\underline{\mathbf{Y}}}$ is a 2×2 matrix the eigenvalues k obtained from (33) are four and they are identical to those obtained from (8). From (33) it is clear that eigenmodes satisfy the $\pm k$ symmetry. They represent two waves that can propagate or attenuate along each positive and negative z-directions, that is, four modes. The characteristic equation of the eigenvalue problem in (33), which represents the dispersion relation of the structure, can be written in their simplest form as

$$k^4 + Tk^2 + D = 0. \tag{34}$$

Therefore, the four roots of the above equation, wavenumbers, can finally be written as in (9).

The eigenvectors of (33) may be written in their simplest form as

$$\mathbf{V}_n = \psi_0\begin{pmatrix} Z_1\left(k_n^2 + Z_2(Y_2+Y_c)\right)\\ Z_1Z_2Y_c\end{pmatrix} \tag{35}$$

where ψ_0 is arbitrary constant, and it has a unit of Am^3. It is important to point about that the eigenvectors representing voltages propagating along the negative z-direction are identical to those in the positive z-direction due to the fact that the structure is reciprocal, however, their corresponding current vectors are not identical to each other, and indeed they have a sign difference, and are determined from (3) as

$$\mathbf{I}_n = jk_n\underline{\underline{\mathbf{Z}}}^{-1}\mathbf{V}_n = \psi_0\begin{pmatrix} jk_n\left(k_n^2 + Z_2(Y_2+Y_c)\right)\\ jZ_1k_nY_c\end{pmatrix}. \tag{36}$$

Combining the eigenvectors in (35) and (36), the four eigenvectors of the eigenvalue problem in (8) are found in their simplest form as in (10)

ACKNOWLEDGMENT

The authors would like to thank DS SIMULIA for providing CST Studio Suite that was instrumental in this study.

REFERENCES

[1] A. Figotin and I. Vitebskiy, "Frozen light in photonic crystals with degenerate band edge," *Phys. Rev. E, Stat. Phys. Plasmas Fluids Relat. Interdiscip. Top.*, vol. 74, no. 6, Dec. 2006, Art. no. 066613.

[2] M. Y. Nada, M. A. K. Othman, and F. Capolino, "Theory of coupled resonator optical waveguides exhibiting high-order exceptional points of degeneracy," *Phys. Rev. B, Condens. Matter*, vol. 96, no. 18, Nov. 2017, Art. no. 184304.

[3] M. A. K. Othman, F. Yazdi, A. Figotin, and F. Capolino, "Giant gain enhancement in photonic crystals with a degenerate band edge," *Phys. Rev. B, Condens. Matter*, vol. 93, no. 2, Jan. 2016, Art. no. 024301.

[4] A. Figotin and I. Vitebskiy, "Gigantic transmission band-edge resonance in periodic stacks of anisotropic layers," *Phys. Rev. E, Stat. Phys. Plasmas Fluids Relat. Interdiscip. Top.*, vol. 72, no. 3, Sep. 2005, Art. no. 036619.

[5] M. Y. Nada, M. A. K. Othman, O. Boyraz, and F. Capolino, "Giant resonance and anomalous quality factor scaling in degenerate band edge coupled resonator optical waveguides," *J. Lightw. Technol.*, vol. 36, no. 14, pp. 3030–3039, Jul. 15, 2018.

[6] A. Figotin and I. Vitebskiy, "Oblique frozen modes in periodic layered media," *Phys. Rev. E, Stat. Phys. Plasmas Fluids Relat. Interdiscip. Top.*, vol. 68, no. 3, Sep. 2003, Art. no. 036609.

[7] H. Kazemi, M. Y. Nada, T. Mealy, A. F. Abdelshafy, and F. Capolino, "Exceptional points of degeneracy induced by linear time-periodic variation," *Phys. Rev. A, Gen. Phys. Appl.*, vol. 11, no. 1, Jan. 2019, Art. no. 014007.

[8] R. El-Ganainy, K. Makris, D. Christodoulides, and Z. H. Musslimani, "Theory of coupled optical PT-symmetric structures," *Opt. Lett.*, vol. 32, no. 17, pp. 2632–2634, 2007.

[9] M. A. K. Othman and F. Capolino, "Theory of exceptional points of degeneracy in uniform coupled waveguides and balance of gain and loss," *IEEE Trans. Antennas Propag.*, vol. 65, no. 10, pp. 5289–5302, Oct. 2017.

[10] G. Mumcu, K. Sertel, and J. L. Volakis, "Miniature antenna using printed coupled lines emulating degenerate band edge crystals," *IEEE Trans. Antennas Propag.*, vol. 57, no. 6, pp. 1618–1624, Jun. 2009.

[11] M. A. K. Othman and F. Capolino, "Demonstration of a degenerate band edge in periodically-loaded circular waveguides," *IEEE Microw. Wireless Compon. Lett.*, vol. 25, no. 11, pp. 700–702, Nov. 2015.

[12] T. Zheng, M. Casaletti, A. F. Abdelshafy, F. Capolino, Z. Ren, and G. Valerio, "Design of substrate integrated waveguides supporting degenerate band-edge resonances," in *Proc. 13th Eur. Conf. Antennas Propag. (EuCAP)*, Krakow, Poland, 2019, pp. 1–3.

[13] C. Locker, K. Sertel, and J. L. Volakis, "Emulation of propagation in layered anisotropic media with equivalent coupled microstrip lines," *IEEE Microw. Wireless Compon. Lett.*, vol. 16, no. 12, pp. 642–644, Dec. 2006.

[14] V. Ananth Tamma, A. Figotin, and F. Capolino, "Concept for pulse compression device using structured spatial energy distribution," *IEEE Trans. Microw. Theory Techn.*, vol. 64, no. 3, pp. 742–755, Mar. 2016.

[15] J. T. Sloan, M. A. K. Othman, and F. Capolino, "Theory of double ladder lumped circuits with degenerate band edge," *IEEE Trans. Circuits Syst. I, Reg. Papers*, vol. 65, no. 1, pp. 3–13, Jan. 2018.

[16] J. R. Burr, N. Gutman, C. M. de Sterke, I. Vitebskiy, and R. M. Reano, "Degenerate band edge resonances in coupled periodic silicon optical waveguides," *Opt. Express*, vol. 21, no. 7, pp. 8736–8745, Apr. 2013.

[17] M. A. K. Othman, X. Pan, G. Atmatzakis, C. G. Christodoulou, and F. Capolino, "Experimental demonstration of degenerate band edge in metallic periodically loaded circular waveguide," *IEEE Trans. Microw. Theory Techn.*, vol. 65, no. 11, pp. 4037–4045, Nov. 2017.

[18] A. F. Abdelshafy, M. A. K. Othman, D. Oshmarin, A. T. Almutawa, and F. Capolino, "Exceptional points of degeneracy in periodic coupled waveguides and the interplay of gain and radiation loss: Theoretical and experimental demonstration," *IEEE Trans. Antennas Propag.*, vol. 67, no. 11, pp. 6909–6923, Nov. 2019.

[19] F. Yazdi, M. A. K. Othman, M. Veysi, A. Figotin, and F. Capolino, "A new amplification regime for traveling wave tubes with third-order modal degeneracy," *IEEE Trans. Plasma Sci.*, vol. 46, no. 1, pp. 43–56, Jan. 2018.

[20] A. F. Abdelshafy, M. A. K. Othman, F. Yazdi, M. Veysi, A. Figotin, and F. Capolino, "Electron-beam-driven devices with synchronous multiple degenerate eigenmodes," *IEEE Trans. Plasma Sci.*, vol. 46, no. 8, pp. 3126–3138, Aug. 2018.

[21] D. Oshmarin *et al.*, "New oscillator concept based on band edge degeneracy in lumped double-ladder circuits," *IET Circuits, Devices Syst.*, vol. 13, no. 7, pp. 950–957, Oct. 2019.

[22] M. Veysi, M. A. K. Othman, A. Figotin, and F. Capolino, "Degenerate band edge laser," *Phys. Rev. B, Condens. Matter*, vol. 97, no. 19, May 2018, Art. no. 195107.

[23] T. Mealy, A. F. Abdelshafy, and F. Capolino, "The degeneracy of the dominant mode in rectangular waveguide," in *Proc. United States Nat. Committee URSI Nat. Radio Sci. Meeting (USNC-URSI NRSM)*, Boulder, CO, USA, 2019, pp. 1–2.

[24] C. M. Bender and S. Boettcher, "Real spectra in non-Hermitian Hamiltonians having PT symmetry," *Phys. Rev. Lett.*, vol. 80, no. 24, p. 5243, 1998.

[25] L. B. Felsen and N. Marcuvitz, *Radiation and Scattering of Waves*. Hoboken, NJ, USA: Wiley, 1994.

[26] N. Marcuvitz and J. Schwinger, "On the representation of the electric and magnetic fields produced by currents and discontinuities in wave Guides. I," *J. Appl. Phys.*, vol. 22, no. 6, pp. 806–819, Jun. 1951.

[27] C. R. Paul, *Analysis of Multiconductor Transmission Lines*. Hoboken, NJ, USA: Wiley, 2008.

[28] G. W. Hanson, A. B. Yakovlev, M. A. K. Othman, and F. Capolino, "Exceptional points of degeneracy and branch points for coupled transmission lines—Linear-algebra and bifurcation theory perspectives," *IEEE Trans. Antennas Propag.*, vol. 67, no. 2, pp. 1025–1034, Feb. 2019.

[29] G. Mumcu, K. Sertel, and J. L. Volakis, "Lumped circuit models for degenerate band edge and magnetic photonic crystals," *IEEE Microw. Wireless Compon. Lett.*, vol. 20, no. 1, pp. 4–6, Jan. 2010.

[30] I. A. Eshrah, A. A. Kishk, A. B. Yakovlev, and A. W. Glisson, "Evanescent rectangular waveguide with corrugated walls: A composite right/left-handed metaguide," *IEEE MTT-S Int. Microw. Symp. Dig.*, Long Beach, CA, Jun. 2005, p. 4.

[31] H. Noh, J.-K. Yang, I. Vitebskiy, A. Figotin, and H. Cao, "Giant resonances near the split band edges of two-dimensional photonic crystals," *Phys. Rev. A, Gen. Phys.*, vol. 82, no. 1, Jul. 2010, Art. no. 013801.

[32] B. Razavi, "A study of phase noise in CMOS oscillators," *IEEE J. Solid-State Circuits*, vol. 31, no. 3, pp. 331–343, Mar. 1996.

[33] A. F. Abdelshafy, D. Oshmarin, M. A. K. Othman, M. M. Green, and F. Capolino, "Distributed degenerate band edge oscillator," 2020, *arXiv:2002.00857*. [Online]. Available: http://arxiv.org/abs/2002.00857

[34] G. V. Eleftheriades, A. K. Iyer, and P. C. Kremer, "Planar negative refractive index media using periodically L-C loaded transmission lines," *IEEE Trans. Microw. Theory Techn.*, vol. 50, no. 12, pp. 2702–2712, Dec. 2002.

[35] C. Caloz and T. Itoh, *Electromagnetic Metamaterials: Transmission Line Theory and Microwave Applications*. Hoboken, NJ, USA: Wiley, 2004.

[36] N. Apaydin, L. Zhang, K. Sertel, and J. L. Volakis, "Experimental validation of frozen modes guided on printed coupled transmission lines," *IEEE Trans. Microw. Theory Techn.*, vol. 60, no. 6, pp. 1513–1519, Jun. 2012.

[37] C. D. Meyer, *Matrix Analysis and Applied Linear Algebra*. Philadelphia, PA, USA: SIAM, 2001.

[38] N. Higham, *Functions of Matrices: Theory and Computation*. Philadelphia, PA, USA: SIAM, 2008.

Tarek Mealy received the B.S. and M.S. degrees in electrical engineering from Cairo University, Cairo, Egypt, in 2013 and 2017, respectively. He is currently pursuing the Ph.D. degree at the Department of Electrical Engineering and Computer Science, University of California at Irvine, Irvine, CA, USA.

His current research interests include multiple interdisciplinary topics in applied/computational electromagnetics, electron beam devices, dispersion engineering of periodic structures, photonics, RF/Microwave circuit and system design, and optical sensors.

Filippo Capolino (Fellow, IEEE) received the Laurea *(cum laude)* and Ph.D. degrees in electrical engineering from the University of Florence, Florence, Italy, in 1993 and 1997, respectively.

From 1997 to 1999, he was a Fulbright and then a Post-Doctoral Fellow with the Department of Aerospace and Mechanical Engineering, Boston University, Boston, MA, USA. From 2000 to 2001, part of 2005 and in 2006, he was a Research Assistant Visiting Professor with the Department of Electrical and Computer Engineering, University of Houston, Houston, TX, USA. In 2002, he became an Assistant Professor with the Department of Information Engineering, University of Siena, Siena, Italy till 2008. He was a Visiting Professor with the Fresnel Institute, Marseille, France, in 2003, and also with the Center de Recherche Paul Pascal, Bordeaux, France, in 2010. Since 2005, he has been the Associate Chair for Graduate Studies in his department. He is currently a Professor with the Department of Electrical Engineering and Computer Science, University of California at Irvine, Irvine, CA, USA. His current research interests include metamaterials and their applications, electron beam devices, antennas, sensors in both microwave and optical ranges, plasmonics, microscopy, wireless systems, millimeter wave chip-integrated antennas and applied electromagnetics in general.

Dr. Capolino received the R. W. P. King Prize Paper Award from the IEEE Antennas and Propagation Society for the Best Paper of the Year 2000, by an author under 36. He was the Founder and the Coordinator of the EU Doctoral Programs on Metamaterials from 2004 to 2009. From 2002 to 2008, he served as an Associate Editor for the IEEE TRANSACTIONS ON ANTENNAS AND PROPAGATION. He is the Editor of the *Metamaterials Handbook* (Boca Raton, FL, USA: CRC Press, 2009).